Electronic Supplementary Material (ESI) for Journal of Materials Chemistry C.

Lead-free Zero Dimensional Tellurium (IV) Chloride-Organic Hybrid with Strong Room Temperature Emission as Luminescent Material

Anupam Biswas,[1,2] Rangarajan Bakthavatsalam,[1,2] Vir Bahadur,[1,2] Chinmoy Biswas,[3] Bhupendra P. Mali,[1,2] Sai Santosh Kumar Raavi,[3] Rajesh G. Gonnade,[1,2] and Janardan Kundu*,[4]

[1,2] CSIR-National Chemical Laboratory, Pune, India.
Academy of Scientific and Innovative Research (AcSIR), Ghaziabad, India.
[3] Indian Institute of Technology Hyderabad, Kandi, India.
[4] Indian Institute of Science Education and Research (IISER) Tirupati, Tirupati, India.

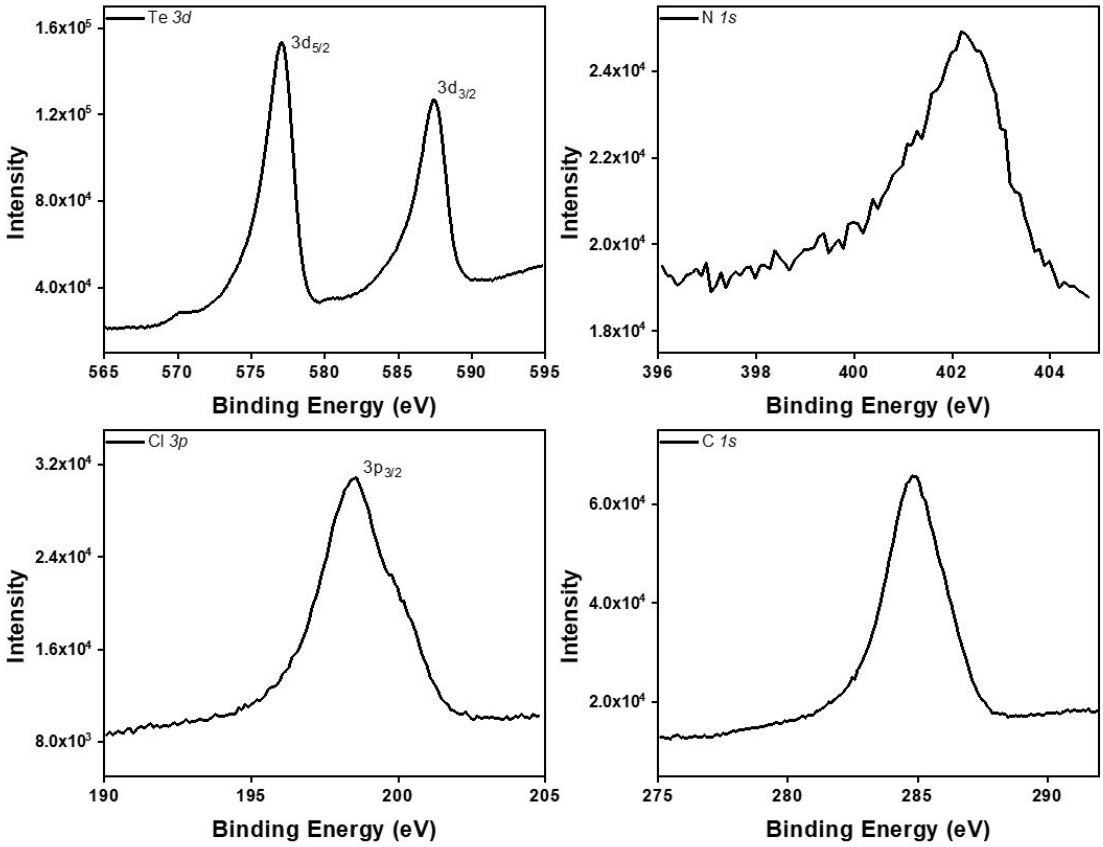

Figure S1: XPS spectra of $(BzTEA)_2TeCl_6$ crystals showing the presence of Chloride anion and Te(IV) metal centre.

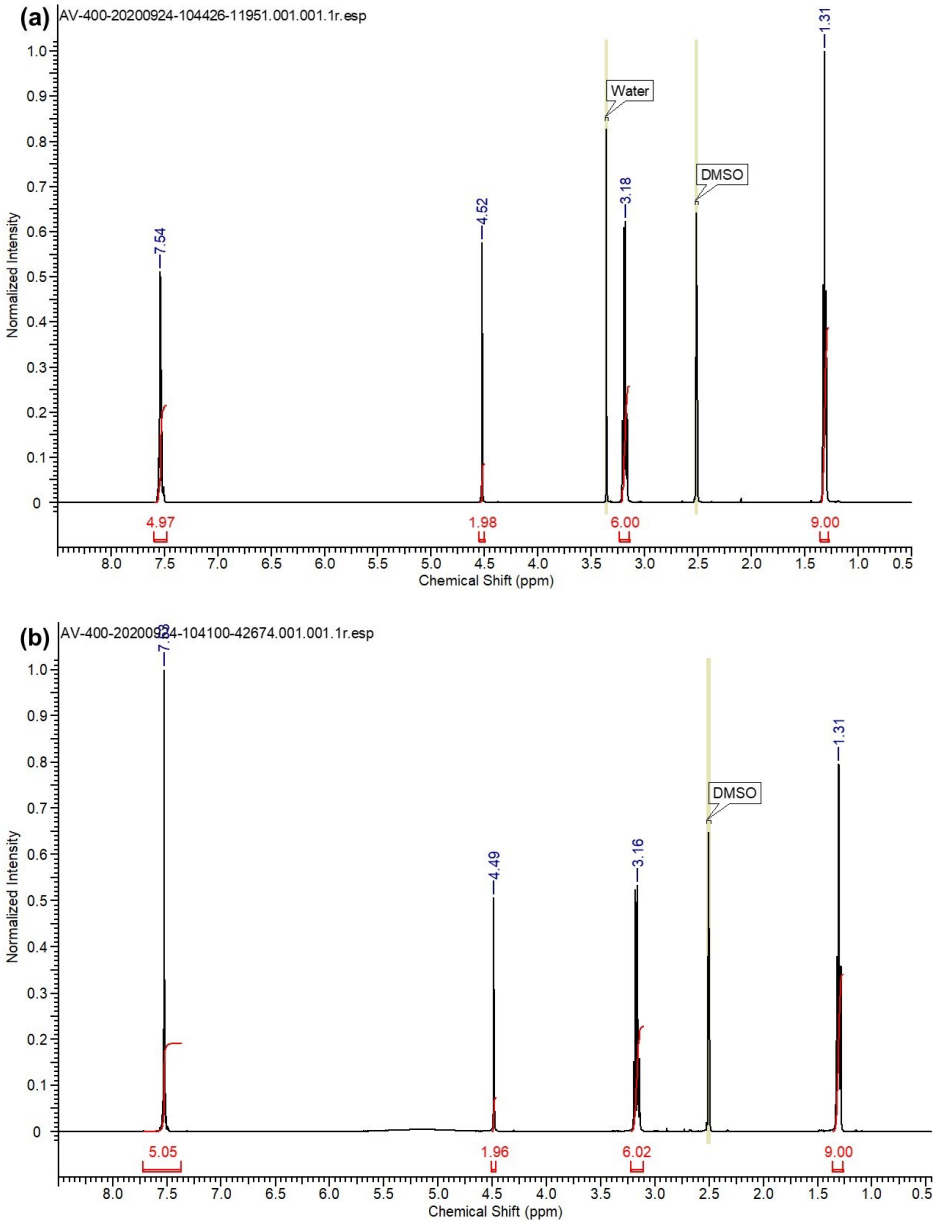

Figure S2: 1H NMR spectra of (a) benzyltriethylammonium chloride and (b) $(BzTEA)_2TeCl_6$ product in DMSO-D6.

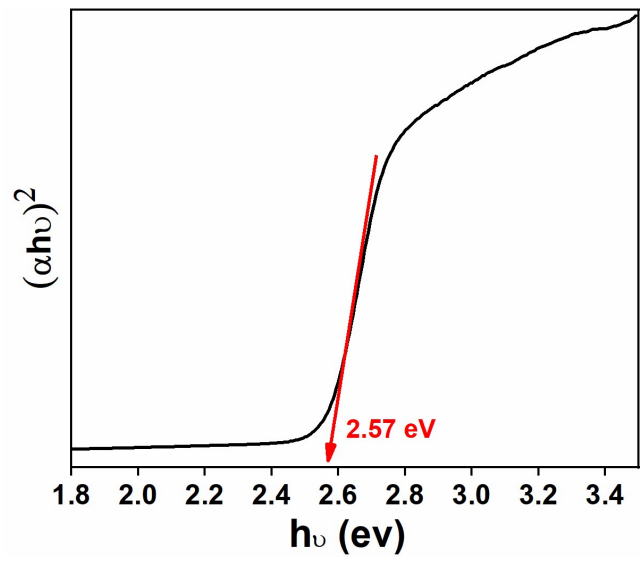

Figure S3: Tauc plot of $(BzTEA)_2TeCl_6$ single crystals showing the direct band gap energy estimation.

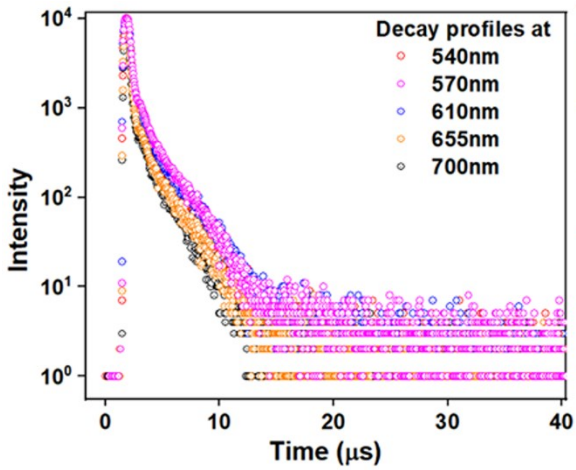

Crystal			
Wavelength (nm)	Lifetime (μs)	Relative %	Average lifetime (μs)
540	1.1	49	8.9
	9.8	51	
570	1.1	42.5	9.13
	9.8	57.5	
610	1.1	44	9.19
	9.9	56	
655	0.8	47.3	8.3
	8.9	52.7	
700	0.7	48.5	7.64
	8.2	51.5	

Figure S4: Lifetime decay profile of $(BzTEA)_2TeCl_6$ crystals collected across the broad emission band when excited with 440 nm source. Table lists the fitted lifetimes, their relative weights and average lifetime.

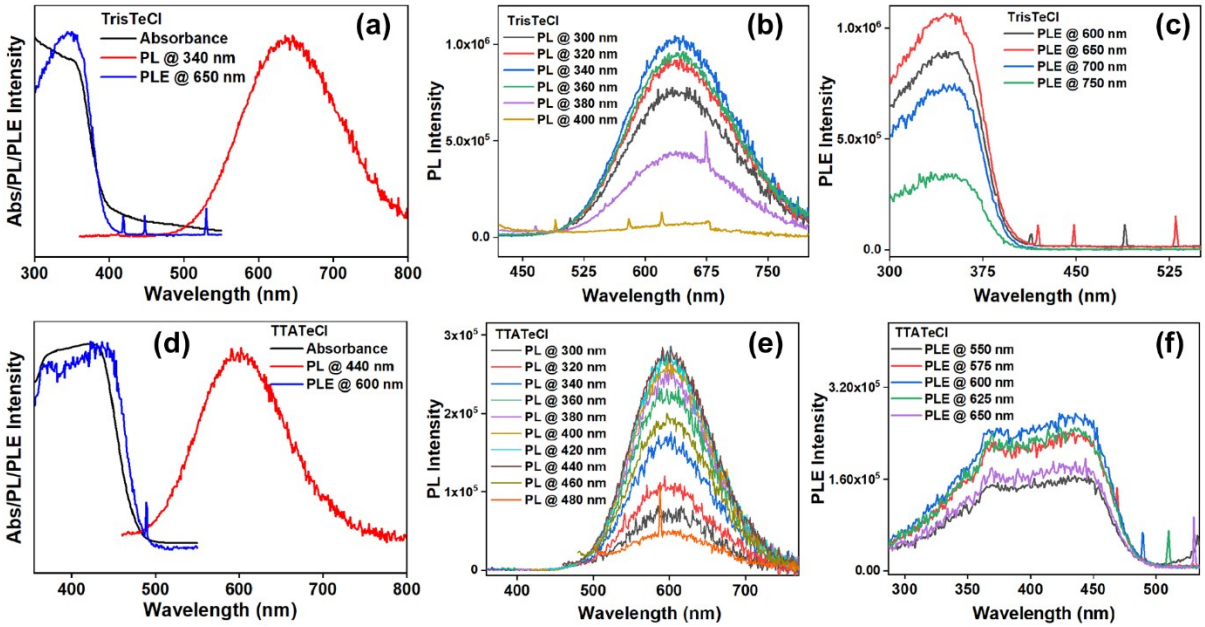

Figure S5: Optical characterization of Te based perovskite with tris(2-aminoethyl)amine (a-c), and tetraethylammonium chloride (d-f) organic ligands showing absorbance, photoluminescence, and photoluminescence excitation, excitation wavelength dependent PL, and PLE across the broad emission band.

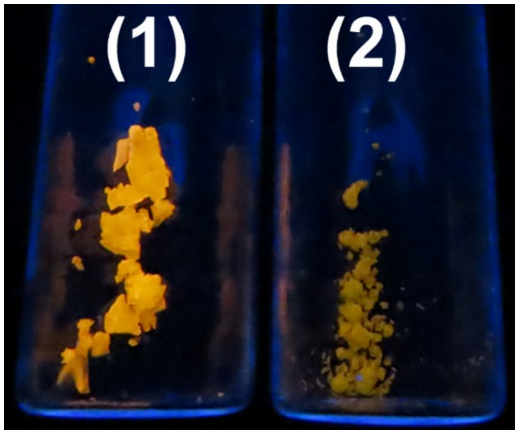

Figure S6: Comparison photograph of Te based perovskite with (1) Benzyltriethylammonium chloride and (2) tetraethylammonium chloride organic ligands under UV illumination.

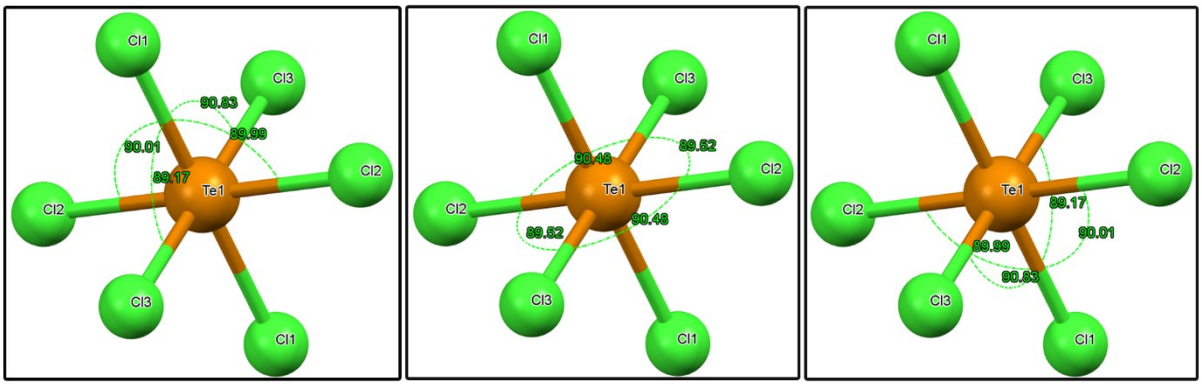

$$\lambda_{\text{oct}} = \frac{1}{6}\sum_{n=1}^{6}\left[\left(d_n - d_0\right)/d_0\right]^2 ; \quad \sigma^2 = \frac{1}{11}\sum_{n=1}^{12}\left(\theta_n - 90^\circ\right)^2$$

Figure S7: Site symmetry of the $TeCl_6$ octahedron showing various bond angles. Mathematical representation of quadratic elongation (λ_{oct}) and bond angle variance (σ^2) is also shown.

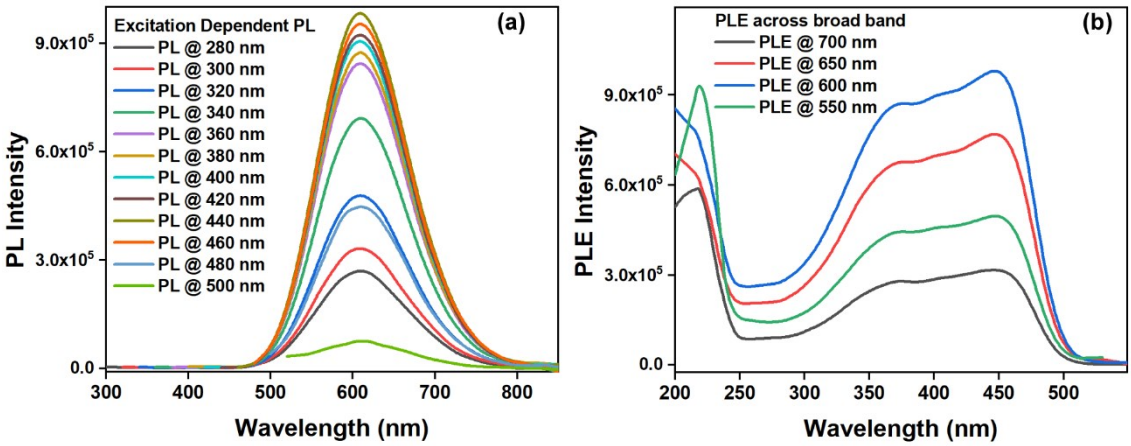

Figure S8: a) Excitation dependent a) PL and b) PLE collected across the broad emission band for $(BzTEA)_2TeCl_6$ crystals.

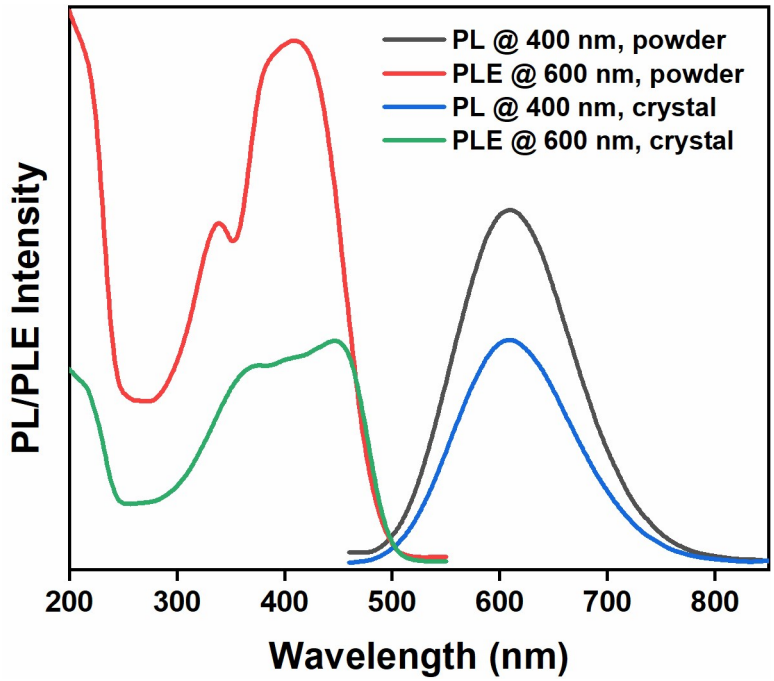

Figure S9: Comparison of the PL and PLE profile for $(BzTEA)_2TeCl_6$ before and after grinding of the crystals.

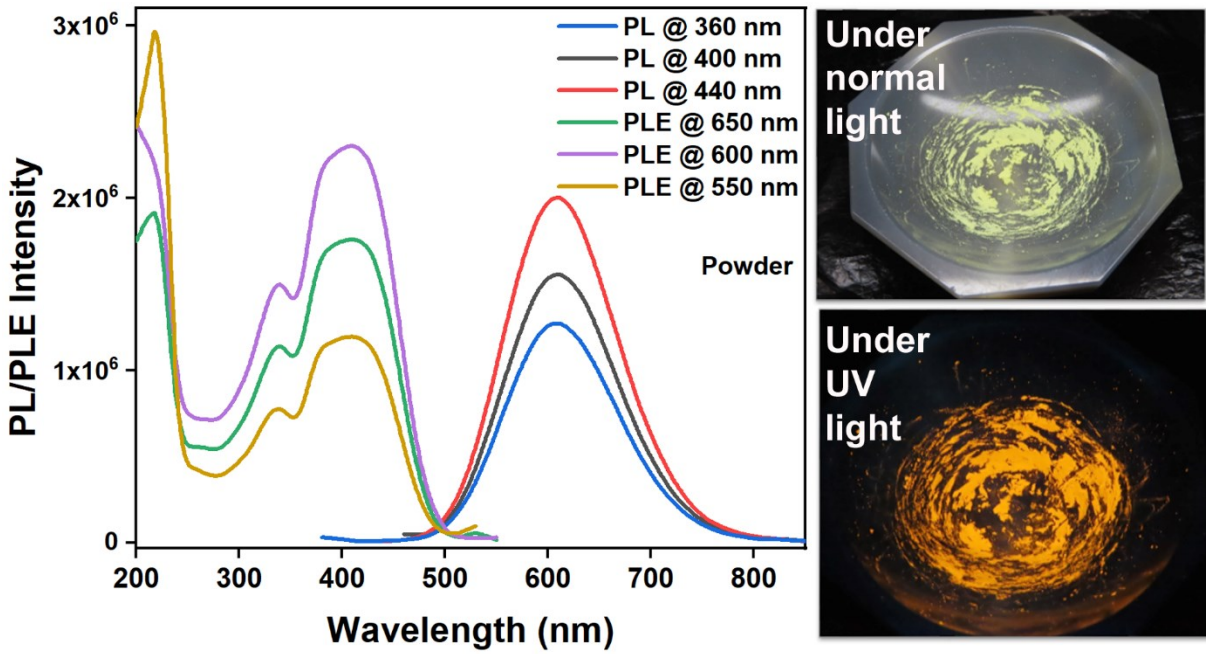

Figure S10: Comparison of the PL and PLE profile for $(BzTEA)_2TeCl_6$ before and after grinding of the crystals along with their images under visible and UV light at room temperature.

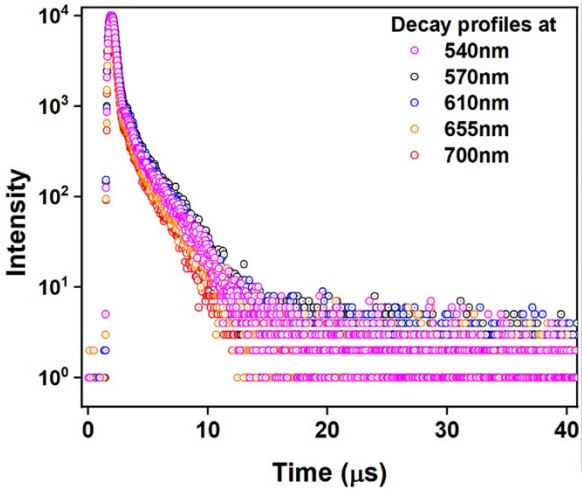

Powder			
Wavelength (nm)	Lifetime (μs)	Relative %	Average lifetime (μs)
540	1.3	58.7	8.36
	9.7	41.3	
570	1.3	52.8	8.9
	10.1	47.2	
610	1.3	53.1	8.2
	9.3	46.9	
655	1.1	58.2	8
	9.2	41.8	
700	1.1	58.5	7.4
	8.6	41.5	

Figure S11: Lifetime decay profile of $(BzTEA)_2TeCl_6$ powder collected across the broad emission band when excited with 440 nm source. Table lists the fitted lifetimes, their relative weights and average lifetime.

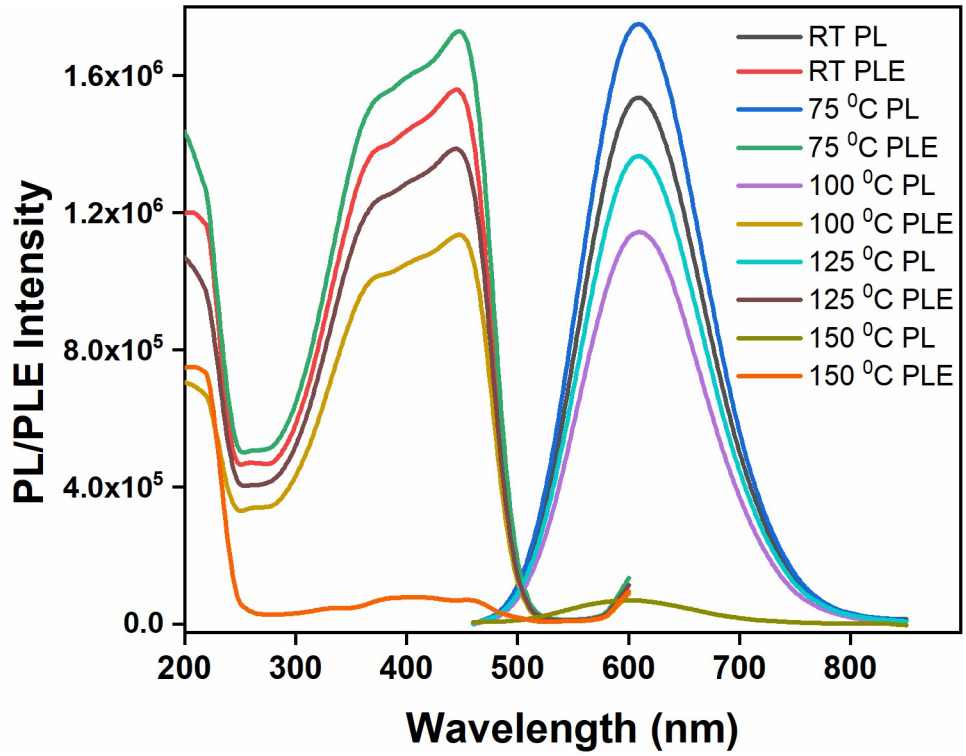

Figure S12: Effect of thermal annealing (from room temperature to 150 °C) of $(BzTEA)_2TeCl_6$ crystals on the PL and PLE profiles. Excitation wavelength for PL is 445 nm and PLE is collected at 610 nm.

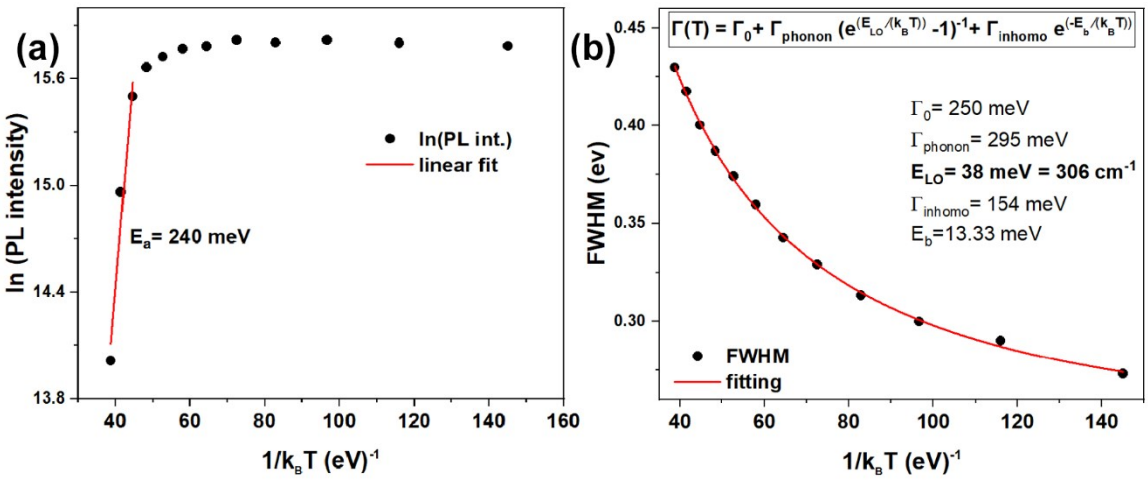

Figure S13: a) Arrhenius plot of natural logarithm of PL intensity against inverse temperature for broad band emission, b) fitting of the bandwidth (FWHM) as a function of temperature

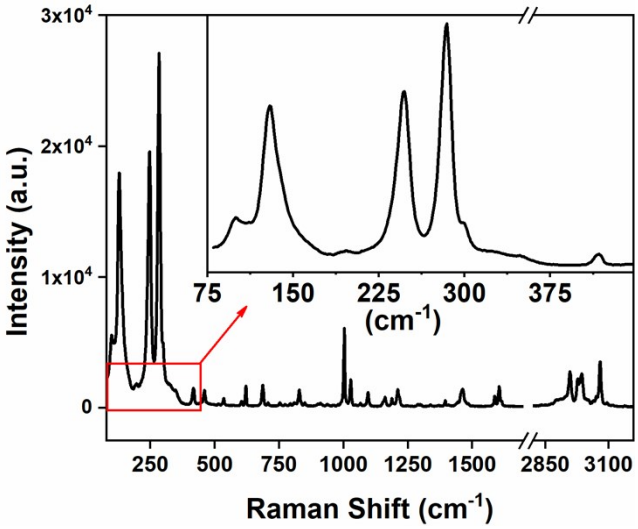

Figure S14: Raman spectra of $(BzTEA)_2TeCl_6$ crystals collected using 633 nm excitation laser source. The inset shows the low frequency phonon modes of the Te-Cl octahedron

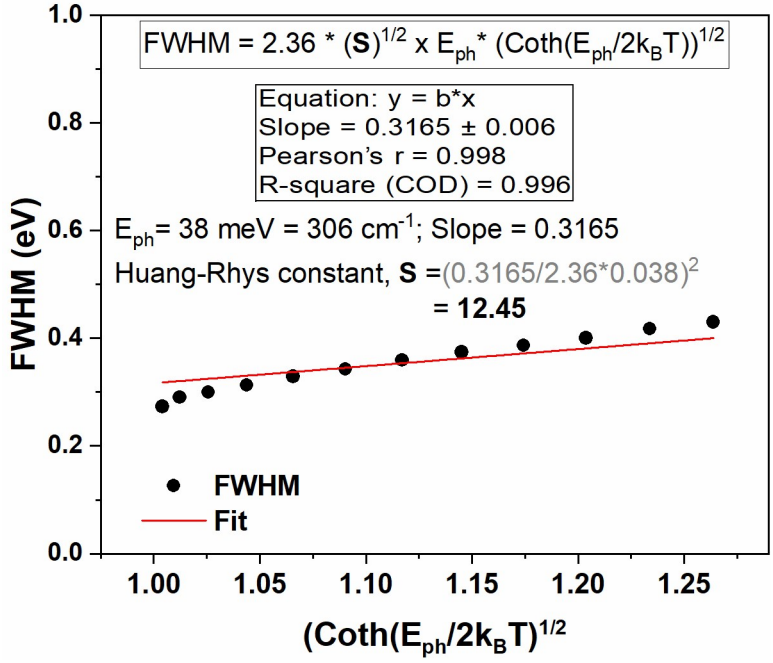

Figure S15: Estimation of Huang-Rhys parameter (**S**) from the temperature dependence of FWHM utilizing the Toyozawa model.

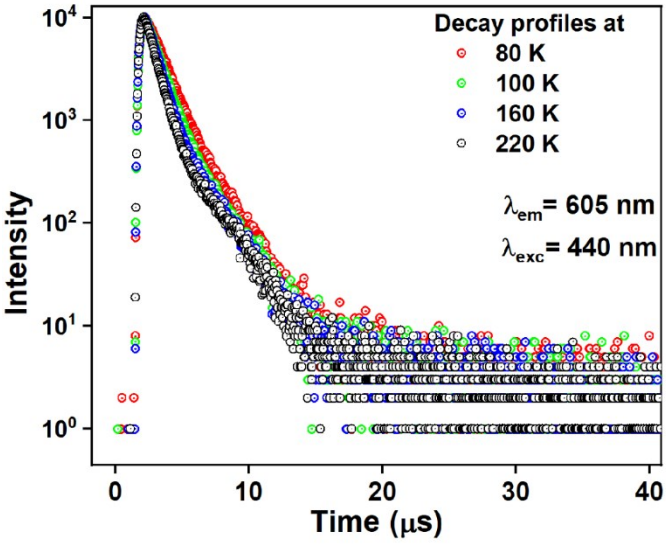

Temperature (K)	Life time (μs)	Relative %
80	6.32	78.6
	12.6	20.6
100	4.98	71.8
	11.8	26.2
160	4.18	68.8
	11.4	30.3
220	2.07	59.6
	10.5	39.1

Figure S16: Lifetime decay profile of $(BzTEA)_2TeCl_6$ crystals collected at low temperatures. Table lists the fitted lifetimes and their relative weights.

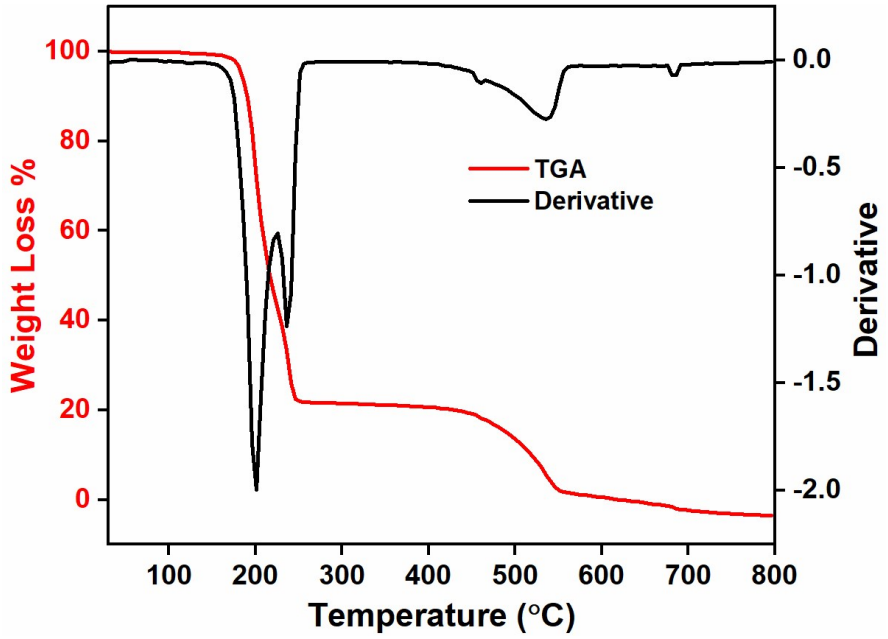

Figure S17: Thermogravimetric weight loss analysis and the derivative of the weight loss curve for $(BzTEA)_2TeCl_6$ crystals.

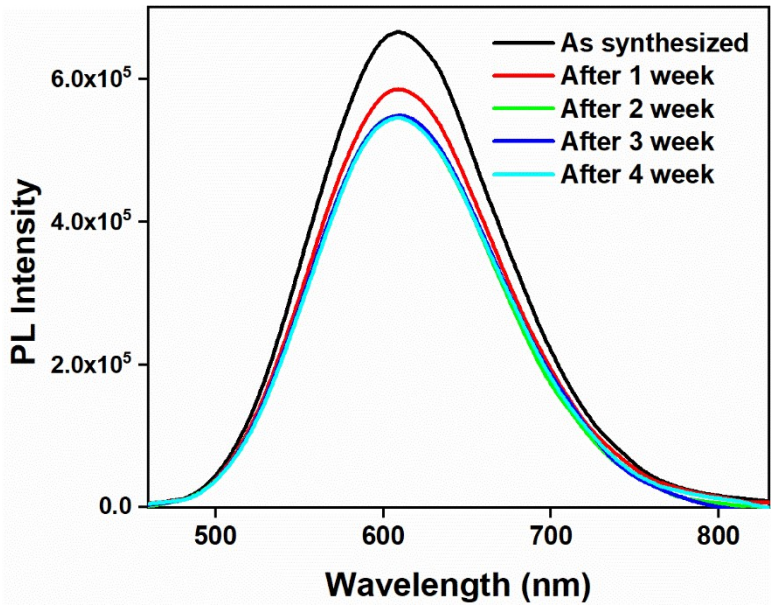

Figure S18: Comparison of PL profile collected (λ_{exc}=440 nm) over time of ambient exposed $(BzTEA)_2TeCl_6$ hybrid

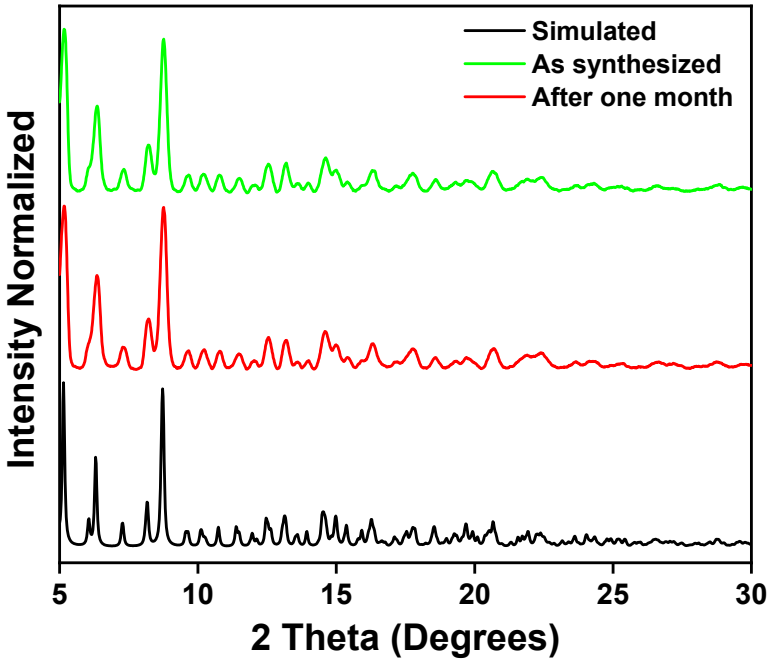

Figure S19: Comparison of PXRD pattern of as synthesized (using Mo source) and after one-month ambient exposure (using Mo source) of $(BzTEA)_2TeCl_6$ hybrid with that of simulated pattern (calculated using Mo source).

Absorbance Peak (nm)	Emission Peak (nm)	Stokes shift (nm)	PLQY (%)	General Formula	Reference
340	400	50	11.52	[(N-AEPz)ZnCl4]Cl	1
370	583	215	86.3	$[Bmim]_2SbCl_5$	2
348	470	122	83	$(C_9NH_{20})_7(PbCl_4)Pb_3Cl_{11}$	3
545	637	128	70	$(bmpy)_9[SbCl_5]_2[Pb_3Cl_{11}]$	4
370, 360	625, 590	250, 245	86, 98	$(TTA)_2SbCl_5$, (TEBA)2$SbCl_5$	5
375	648	273	87	$(Ph_4P)_2SbCl_5$	6
348	512	164	Near unity	$(bmpy)_9[ZnCl_4]_2[Pb_3Cl_{11}]$	7
370	670	300	3	$(C_4H_{14}N_2)_2In_2Br_{10}$	8
365	610	245	35	$(PMA)_3InBr_6$	9
375	450	75	50	$(C_6N_2H_{16}Cl)_2SnCl_6$	10
355, 410, 380	570, 620, 590	215, 210, 210	95, 75, 98	$(C_4N_2H_{14}Br)_4SnBr_6$, $(C_4N_2H_{14}I)_4SnI_6$, $(C_9NH_{20})_2SbCl_5$	11
448	608	160	15	Our system: $(BzTEA)_2TeCl_6$	

Table S1. Comparison of optical properties of various lead-free 0D system

Table S2. Comparison of optical properties of various Te based hybrid systems (Ref 12,13)

Absorption edge (nm)	Emission Peak (nm)	General Formula
545	610	$(NH_4)_2TeCl_6$
560	No emission	$(CH_3NH_3)_2TeCl_6$
545	615	$((CH_3)_2NH_2)_2TeCl_6$
550	No emission	$((CH_3)_3NH)_2TeCl_6$
550	605	$((CH_3)_4N)_2TeCl_6$
510	605	$((C_2H_5)_2NH_2)_2TeCl_6$
555	610	$((C_2H_5)_3NH)_2TeCl_6$
540	580	$((C_2H_5)_4N)_2TeCl_6$
570	605	$((C_4H_9)_4N)_2TeCl_6$
510	580	$(HGu)_2TeCl_6$
490	600	$(HDphg)_2TeCl_6$

490	570	$(HDip)_2TeCl_6$
510	605	$(HPhen)_2TeCl_6$
515	608	**This Work**: $(BzTEA)_2TeCl_6$

References

1. X. Zhang, L. Li, S. Wang, X. Liu, Y. Yao, Y. Peng, M. Hong and J. Luo, *Inorg. Chem*., 2020, **59**, 3527-3531.
2. Z. P. Wang, J. Y. Wang, J. R. Li, M. L. Feng, G. D. Zou and X. Y. Huang, *Chem. Commun*., 2015, **51**, 3094-3097.
3. C. Zhou, H. Lin, M. Worku, J. Neu, Y. Zhou, Y. Tian, S. Lee, P. Djurovich, T. Siegrist and B. Ma, *J.Am.Chem.Soc*., 2018,**140**, 13181-13184.
4. C. Zhou, S. Lee, H. Lin, J. Neu, M. Chaaban, L.-J. Xu, A. Arcidiacono, Q. He, M. Worku, L. Ledbetter, X. Lin, J. A. Schlueter, T. Siegrist and B. Ma, *ACS Materials Letters*, 2020, 2, 376-380.
5. Z. Li, Y. Li, P. Liang, T. Zhou, L. Wang and R.-J. Xie, *Chem. Mater*., 2019, **31**, 9363-9371.
6. C. Zhou, M. Worku, J. Neu, H. Lin, Y. Tian, S. Lee, Y. Zhou, D. Han, S. Chen, A. Hao, P. I. Djurovich, T. Siegrist, M.-H. Du and B. Ma, *Chem. Mater*., 2018, **30**, 2374-2378.
7. C. Zhou, H. Lin, J. Neu, Y. Zhou, M. Chaaban, S. Lee, M. Worku, B. Chen, R. Clark, W. Cheng, J. Guan, P. Djurovich, D. Zhang, X. Lü, J. Bullock, C. Pak, M. Shatruk, M.-H. Du, T. Siegrist and B. Ma, *ACS Energy Letters*, 2019, **4**, 1579-1583.
8. A. Yangui, R. Roccanova, T. M. McWhorter, Y. Wu, M.-H. Du and B. Saparov, *Chem. Mater*., 2019, **31**, 2983-2991.
9. L. Zhou, J. F. Liao, Z. G. Huang, J. H. Wei, X. D. Wang, H. Y. Chen and D. B. Kuang, *Angew. Chem.* , 2019, **58**, 15435-15440.
10. G. Song, M. Li, Y. Yang, F. Liang, Q. Huang, X. Liu, P. Gong, Z. Xia and Z. Lin*, J. Phys. Chem. Lett*., 2020, **11**, 1808-1813.
11. C. Zhou, H. Lin, Y. Tian, Z. Yuan, R. Clark, B. Chen, L. J. van de Burgt, J. C. Wang, Y. Zhou, K. Hanson, Q. J. Meisner, J. Neu, T. Besara, T. Siegrist, E. Lambers, P. Djurovich and B. Ma, *Chem. Sci*., 2018, **9**, 586-593.
12. T. V. Sedakova and A. G. Mirochnik, *Opt. Spectrosc.*, 2015, **119**, 54-58.

T. V. Sedakova, A. G. Mirochnik and V. E. Karasev, *Opt. Spectrosc.*, 2011, **110**, 755-761.

Single crystal Data:

X-ray intensity data measurements of compound **$(BzTEA)_2TeCl_6$** was carried out on a Bruker D8 VENTURE Kappa Duo PHOTON II CPAD diffractometer equipped with Incoatech multilayer mirrors optics. The intensity measurements were carried out with Mo micro-focus sealed tube diffraction source (MoK_α= 1.54178 Å) at 100(2) K temperature. The X-ray generator was operated at 50 kV and 1.4 mA. A preliminary set of cell constants and an orientation matrix were calculated from three matrix sets of 36 frames (each matrix run consists

of 12 frames). Data were collected with ω scan width of 0.5° at different settings of φ and 2θ with a frame time of 15 secs keeping the sample-to-detector distance fixed at 5.00 cm. The X-ray data collection was monitored by APEX3 program (Bruker, 2016).[1] All the data were corrected for Lorentzian, polarization and absorption effects using SAINT and SADABS programs (Bruker, 2016). Using the APEX3 (Bruker) program suite, the structure was solved with the ShelXS-97 (Sheldrick, 2008)[2] structure solution program, using direct methods. The model was refined with a version of ShelXL-2018/3 (Sheldrick, 2015)[3] using Least Squares minimization. All the hydrogen atoms were placed in a geometrically idealized position and constrained to ride on its parent atoms.

Data for $(BzTEA)_2TeCl_6$: A single crystal of compound **$(BzTEA)_2TeCl_6$**, molecular formula $2(C_{13}H_{22}N)$ $TeCl_6$, approximate dimensions 0.019 mm x 0.071 mm x 0.079 mm, was used for the X-ray crystallographic analysis. The X-ray intensity data were measured (λ = 0.71073 Å). The integration of the data using a monoclinic unit cell yielded a total of 40868 reflections to a maximum θ angle of 27.99° (0.76 Å resolution), of which 3894 were independent (average redundancy 10.495, completeness = 99.8%, R_{int} = 5.90%, R_{sig} = 2.59%) and 3378 (86.75%) were greater than $2\sigma(F^2)$. The final cell constants of a = 11.2243(5) Å, b = 11.1763(5) Å, c =12.9134(6) Å, β = 90.737(2)°, volume = 1619.80(13) Å^3, are based upon the refinement of the XYZ-centroids of reflections above 20 σ(I). The calculated minimum and maximum transmission coefficients (based on crystal size) are 0.8950 and 0.9730. The structure was solved and refined using the Bruker SHELXTL Software Package, using the space group $P2_1/n$, with Z = 2 for the formula unit, $2(C_{13}H_{22}N)$ $TeCl_6$. The final anisotropic full-matrix least-squares refinement on F^2 with 163 variables converged at R1 = 2.84%, for the observed data and wR2 = 7.28% for all data. The goodness-of-fit was 1.123. The largest peak in the final difference electron density synthesis was 0.826 e^-

/Å^3 and the largest hole was -0.420 e$^-$/Å^3 with an RMS deviation of 0.094 e$^-$/Å^3. On the basis of the final model, the calculated density was 1.486 g/cm^3 and F(000), 736 e$^-$.

Table S3. Crystal data for $(BzTEA)_2TeCl_6$

Identification code	$(BzTEA)_2TeCl_6$	
Chemical formula	$C_{13}H_{22}Cl_3NTe_{0.50}$	
Formula weight	362.46 g/mol	
Temperature	100(2) K	
Wavelength	0.71073 Å	
Crystal size	0.019 x 0.071 x 0.079 mm	
Crystal system	monoclinic	
Space group	$P2_1/n$	
Unit cell dimensions	a = 11.2243(5) Å	α = 90°
	b = 11.1763(5) Å	β = 90.737(2)°
	c = 12.9134(6) Å	γ = 90°
Volume	1619.80(13) Å^3	
Z	2	
Density (calculated)	1.486 g/cm^3	
Absorption coefficient	1.431 mm^{-1}	
F(000)	736	
Theta range for data collection	2.39 to 27.99°	
Index ranges	-14<=h<=14, -14<=k<=14, -17<=l<=17	
Reflections collected	40868	
Independent reflections	3894 [R(int) = 0.0590]	
Max. and min. transmission	0.9730 and 0.8950	
Structure solution technique	direct methods	
Structure solution program	SHELXT 2014/5 (Sheldrick, 2014)	
Refinement method	Full-matrix least-squares on F^2	
Refinement program	SHELXL-2018/3 (Sheldrick, 2018)	

Function minimized	$\Sigma\ w(F_o^2 - F_c^2)^2$	
Data / restraints / parameters	3894 / 0 / 163	
Goodness-of-fit on F^2	1.123	
Δ/σ_{max}	0.001	
Final R indices	3378 data; $I>2\sigma(I)$	R1 = 0.0284, wR2 = 0.0633
	all data	R1 = 0.0383, wR2 = 0.0728
Weighting scheme	$w=1/[\sigma^2(F_o^2)+(0.0190P)^2+3.4895P]$ where $P=(F_o^2+2F_c^2)/3$	
Largest diff. peak and hole	0.826 and -0.420 $eÅ^{-3}$	
R.M.S. deviation from mean	0.094 $eÅ^{-3}$	

Table S4. Bond lengths (Å) for $(BzTEA)_2TeCl_6$

Te1-Cl2	2.5241(6)	Te1-Cl2#1	2.5241(6)
Te1-Cl3	2.5302(6)	Te1-Cl3#1	2.5302(6)
Te1-Cl1#1	2.5487(6)	Te1-Cl1	2.5487(6)
N1-C8	1.511(3)	N1-C10	1.516(4)
N1-C12	1.531(3)	N1-C1	1.534(3)
C1-C2	1.507(4)	C1-H1A	0.99
C1-H1B	0.99	C2-C3	1.396(4)
C2-C7	1.397(4)	C3-C4	1.384(4)
C3-H3	0.95	C4-C5	1.389(4)
C4-H4	0.95	C5-C6	1.383(5)
C5-H5	0.95	C6-C7	1.379(4)
C6-H6	0.95	C7-H7	0.95
C8-C9	1.525(4)	C8-H8A	0.99
C8-H8B	0.99	C9-H9A	0.98
C9-H9B	0.98	C9-H9C	0.98
C10-C11	1.513(4)	C10-H10A	0.99
C10-H10B	0.99	C11-H11A	0.98
C11-H11B	0.98	C11-H11C	0.98
C12-C13	1.516(4)	C12-H12A	0.99
C12-H12B	0.99	C13-H13A	0.98
C13-H13B	0.98	C13-H13C	0.98

Symmetry transformations used to generate equivalent atoms:
#1 $-x+1, -y+2, -z+1$

Table S5. Bond angles (°) for $(BzTEA)_2TeCl_6$.

Cl2-Te1-Cl2#1	180.00(3)	Cl2-Te1-Cl3	89.52(2)
Cl2#1-Te1-Cl3	90.48(2)	Cl2-Te1-Cl3#1	90.48(2)
Cl2#1-Te1-Cl3#1	89.52(2)	Cl3-Te1-Cl3#1	180.0
Cl2-Te1-Cl1#1	90.01(2)	Cl2#1-Te1-Cl1#1	89.99(2)
Cl3-Te1-Cl1#1	89.17(2)	Cl3#1-Te1-Cl1#1	90.83(2)
Cl2-Te1-Cl1	89.99(2)	Cl2#1-Te1-Cl1	90.01(2)
Cl3-Te1-Cl1	90.83(2)	Cl3#1-Te1-Cl1	89.17(2)
Cl1#1-Te1-Cl1	180.0	C8-N1-C10	112.0(2)
C8-N1-C12	106.9(2)	C10-N1-C12	110.8(2)
C8-N1-C1	111.2(2)	C10-N1-C1	105.6(2)
C12-N1-C1	110.4(2)	C2-C1-N1	115.8(2)
C2-C1-H1A	108.3	N1-C1-H1A	108.3
C2-C1-H1B	108.3	N1-C1-H1B	108.3
H1A-C1-H1B	107.4	C3-C2-C7	118.0(3)
C3-C2-C1	120.8(3)	C7-C2-C1	121.1(3)
C4-C3-C2	121.1(3)	C4-C3-H3	119.5
C2-C3-H3	119.5	C3-C4-C5	119.7(3)
C3-C4-H4	120.1	C5-C4-H4	120.1
C6-C5-C4	120.0(3)	C6-C5-H5	120.0
C4-C5-H5	120.0	C7-C6-C5	120.0(3)
C7-C6-H6	120.0	C5-C6-H6	120.0
C6-C7-C2	121.2(3)	C6-C7-H7	119.4
C2-C7-H7	119.4	N1-C8-C9	115.1(3)
N1-C8-H8A	108.5	C9-C8-H8A	108.5
N1-C8-H8B	108.5	C9-C8-H8B	108.5
H8A-C8-H8B	107.5	C8-C9-H9A	109.5
C8-C9-H9B	109.5	H9A-C9-H9B	109.5
C8-C9-H9C	109.5	H9A-C9-H9C	109.5
H9B-C9-H9C	109.5	C11-C10-N1	115.2(2)
C11-C10-H10A	108.5	N1-C10-H10A	108.5
C11-C10-H10B	108.5	N1-C10-H10B	108.5

H10A-C10-H10B	107.5	C10-C11-H11A	109.5
C10-C11-H11B	109.5	H11A-C11-H11B	109.5
C10-C11-H11C	109.5	H11A-C11-H11C	109.5
H11B-C11-H11C	109.5	C13-C12-N1	115.0(2)
C13-C12-H12A	108.5	N1-C12-H12A	108.5
C13-C12-H12B	108.5	N1-C12-H12B	108.5
H12A-C12-H12B	107.5	C12-C13-H13A	109.5
C12-C13-H13B	109.5	H13A-C13-H13B	109.5
C12-C13-H13C	109.5	H13A-C13-H13C	109.5
H13B-C13-H13C	109.5		

Symmetry transformations used to generate equivalent atoms:
#1 -x+1, -y+2, -z+1

Table S6. Torsion angles (°) for $(BzTEA)_2TeCl_6$.

C8-N1-C1-C2	-58.1(3)	C10-N1-C1-C2	-179.8(2)
C12-N1-C1-C2	60.4(3)	N1-C1-C2-C3	92.8(3)
N1-C1-C2-C7	-91.8(3)	C7-C2-C3-C4	0.8(4)
C1-C2-C3-C4	176.4(3)	C2-C3-C4-C5	0.0(4)
C3-C4-C5-C6	0.4(5)	C4-C5-C6-C7	-1.8(5)
C5-C6-C7-C2	2.6(5)	C3-C2-C7-C6	-2.1(5)
C1-C2-C7-C6	-177.7(3)	C10-N1-C8-C9	51.8(3)
C12-N1-C8-C9	173.3(3)	C1-N1-C8-C9	-66.1(3)
C8-N1-C10-C11	59.0(3)	C12-N1-C10-C11	-60.4(3)
C1-N1-C10-C11	-179.8(2)	C8-N1-C12-C13	-174.3(2)
C10-N1-C12-C13	-52.0(3)	C1-N1-C12-C13	64.6(3)

References

1. Bruker (2016). APEX2, SAINT and SADABS. Bruker AXS Inc., Madison, Wisconsin, USA.
2. G. M. Sheldrick, *Acta Crystallogr.*, 2008, A64, 112.
3. G. M. Sheldrick, *Acta Crystallogr.*, 2015, C71, 3–8.
4. L. J. Farrugia, *J. Appl. Crystallogr.* 2012, 45, 849–854.